

Transcutaneous Measurement of Essential Vitamins Using Near-Infrared Fluorescent Single-Walled Carbon Nanotube Sensors

Naveed A. Bakh, Xun Gong, Michael A. Lee, Xiaojia Jin, Volodymyr B. Koman, Minkyung Park, Freddy T. Nguyen, and Michael S. Strano*

Vitamins such as riboflavin and ascorbic acid are frequently utilized in a range of biomedical applications as drug delivery targets, fluidic tracers, and pharmaceutical excipients. Sensing these biochemicals in the human body has the potential to significantly advance medical research and clinical applications. In this work, a nanosensor platform consisting of single-walled carbon nanotubes (SWCNTs) with nanoparticle corona phases engineered to allow for the selective molecular recognition of ascorbic acid and riboflavin, is developed. The study provides a methodological framework for the implementation of colloidal SWCNT nanosensors in an intraperitoneal SKH1-E murine model by addressing complications arising from tissue absorption and scattering, mechanical perturbations, as well as sensor diffusion and interactions with the biological environment. Nanosensors are encapsulated in a polyethylene glycol diacrylate hydrogel and a diffusion model is utilized to validate analyte transport and sensor responses to local concentrations at the boundary. Results are found to be reproducible and stable after exposure to 10% mouse serum even after three days of *in vivo* implantation. A geometrical encoding scheme is used to reference sensor pairs, correcting for *in vivo* optical and mechanical artifacts, resulting in an order of magnitude improvement of *p*-value from 0.084 to 0.003 during analyte sensing.

measurements is the continuous glucose monitors (CGMs) for the management of blood glucose in diabetics.^[7,8] While with CGM, chemical measurement significantly improved patient outcomes,^[9] the development of molecule specific sensor elements often occurs on a case-by-case basis.

There has been significant interest in developing sensors that can operate within the human body, communicating information on the human endocrine system, steroidogenesis hormone signaling,^[10] and drug efficacy.^[11] As analytes, vitamins such as riboflavin and ascorbic acid are frequently utilized in a range of biomedical applications as drug delivery targets in and of themselves,^[12,13] tracers for physiological fluid flow,^[14] and as pharmaceutical excipients.^[15,16] The ability for sensor technology to detect these important biochemicals in the human body has the potential to significantly advance medical research for clinical applications.


In recent years, fluorescent single walled carbon nanotubes (SWCNTs) have shown promise as continuous fluorescent sensors.^[17–19] SWCNT near-infrared (nIR) emission is useful for biological sensing as it occurs within the tissue penetration window where optical absorption is at a minimum.^[18–20] SWCNT fluorescence also does not photobleach with repeated query, making it suitable for long term monitoring.^[17,18,21] As SWCNTs are hydrophobic, amphiphilic coronas are necessary to disperse them in aqueous environments to enable their optical properties.^[22,23] Depending on the engineered corona phase around the nanoparticle, analytes can selectively interact with the colloidal SWCNTs to modulate their nIR emission photoluminescence (PL) intensity or wavelength.^[23] This phenomena is known as corona phase molecular recognition (CoPhMoRe) and can form the basis of sensors design.^[23] To date, CoPhMoRe sensors have been developed for multiple classes of analytes including small molecules,^[24–29] lipids,^[30] nucleic acids,^[31] and proteins.^[32,33]

CoPhMoRe sensors have been applied in several *in vivo* cases. They can monitor plant root uptake of analytes by immobilizing the sensors within the leaf mesophyll.^[34] In human tissues, SWCNT sensors have been used in brain tissue to detect

1. Introduction

Information retrieved from *in vivo* imaging modalities can be roughly divided into structural versus functional categories. Examples of traditional techniques that detect pathological processes from abnormal anatomical changes include CT (computed tomography),^[1] OCT (optical coherence tomography),^[2] and MRI (magnetic resonance imaging).^[3] In contrast, functional imaging taps the ability to detect chemicals, proteins, nucleic acids, and other molecules to inform on the causes of dysfunction.^[4–6] One widely utilized example of functional

Dr. N. A. Bakh, Dr. X. Gong, Dr. M. A. Lee, X. Jin, Dr. V. B. Koman, M. Park, Dr. F. T. Nguyen, Prof. M. S. Strano
Department of Chemical Engineering
Massachusetts Institute of Technology
77 Massachusetts Ave., Cambridge, MA 02139, USA
E-mail: strano@mit.edu

 The ORCID identification number(s) for the author(s) of this article can be found under <https://doi.org/10.1002/sml.202100540>.

DOI: 10.1002/sml.202100540

neurotransmitters.^[35] In murine tissue, SWCNT sensors have been injected to detect nitric oxide,^[36] miRNA,^[31] chemotherapeutics,^[11] and lipids.^[30] Additionally, these SWCNT sensors show stability in vivo over many months suggesting their feasibility as long-term reporters.^[30,36,37]

However, targeted implantation and transcutaneous measurements present additional nanosensor design and fabrication challenges. This can be subcategorized into error attributed to sensor movement or tissue factors. The former involves the previous cases where sensor particles are injected directly into tissues,^[11,37,39] where the sensor responses can be obfuscated by emitter physical transport overtime. The latter involves the method error from factors such as breathing, heart beat, or other voluntary disturbances.^[38] One solution is using a wavelength shift based SWCNT sensor,^[30] which is agnostic to fluorescence intensity changes.

For intensity change-based SWCNT sensors, a common approach is to ratiometrically normalize sensor signals to a non-responding reference. This can correct sensor movement as well as hardware contributed fluctuations. The usual implementation of this method involves introducing multiple fluorophores with non-overlapping emission wavelengths.^[40] An alternative approach is spatial encoding, where sensor and reference are physically placed in proximity and image processing is used for ratiometric correction. Advantages of this latter method include the relatively simpler optical hardware as well as relative improvements in signal strength or temporal resolution. We have successfully implemented this strategy previously in plants.^[33,41]

In this work, we introduce and study near-infrared fluorescent sensors for riboflavin (Vitamin B2) and ascorbic acid (Vitamin C), and then use them to solve engineering challenges associated with their in vivo implantation, noise sources, and signal stability. First, DNA-wrapped SWCNTs were optimized to selectively detect riboflavin or ascorbic acid. With the help of transport modeling, we develop a hydrogel encapsulation system to limit colloidal sensor diffusion. The resulting sensor gel can be stably and reproducibly queried in biological environments. Next, we utilize spatial encoding to ratiometrically correct for movement-based mechanical artifacts. The overall system is tested using controlled injections in vivo. The results demonstrated successful removal of experimental noise sources, enabling successful intraperitoneal in vivo optical readouts.

2. Results and Discussion

2.1. Sensor Characterization

To test our proposed ratio metric in vivo sensing system, sensor-analyte pairs need to be chosen such that the analyte can be both administered and detected at high doses without causing harm to the test animal. Riboflavin and ascorbic acid are relatively safe and have known modulation of DNA-wrapped SWCNT optical signal.^[42] CoPhMoRe sensors are first tested for optical response against likely interferents. We use a screen of a library of DNA-wrapped SWCNTs against a panel of small molecules to choose the candidates with the best relative

selectivity (See “Biomolecular Screen” in Supporting Information for additional information).

Using 100 μM analyte incubations, we found SWCNTs wrapped with (ACCA)₇ DNA show a 100% increase in PL emission in response to ascorbic acid and those wrapped with (AC)₁₅ DNA show a 90% decrease in PL emission in response to riboflavin. nIR PL emission spectra with concentration titration is shown in **Figure 1A,C**. To further characterize our sensor candidates, we modeled the sensor analyte interaction as a cooperative equilibrium.

First, the sensor response is normalized to control:

$$R = \frac{I}{I_0} \quad (1)$$

where R is the response to analyte, I is fluorescence at each condition, and I_0 is the initial fluorescence before analyte addition. Calibration curves using R (**Figure 1B,D**) can be constructed and fit by a cooperative equilibrium model as described previously:^[28]

$$\frac{I}{I_0} = a \frac{C^n}{K_D^n + C^n} + 1 \quad (2)$$

where n is a cooperativity coefficient, a is a proportionality constant to convert concentration to fluorescence, K_D is the dissociation constant, and C is the concentration of analyte bound. The fitted parameters for the solution phase calibration curves are shown in **Table 1**. The strong intensity modulation proportionality constants, a , observed make these sensors ideal candidates for the subsequent study.

2.2. Hydrogel Design and Synthesis

To prevent diffusive movement error, we localize the colloidal SWCNT sensors in a hydrogel implant. This enabled higher confidence in multiple sensor queries for long-term monitoring. For such a hydrogel sensing system, there are several transport requirements. The cross-linking density should be such that the nanoparticle sensors do not diffuse or leach out significantly during the course of an experiment. The implant also needs to be porous enough for the analyte of interest to diffuse in and interact with the sensors on the order of minutes for adequate response time. Finally, the chemical composition of the implant itself needs to have minimal impact on sensor performance and ideally provides protection to the DNA-SWCNTs against interfering molecules found in the complex in vivo environment.^[43]

Previously, we embedded SWCNTs in alginate hydrogels for in vivo implantation and have shown PL emission stability over hundreds of days.^[36] However, sensor response still needs to be evaluated in any new hydrogel system. Polyethylene glycol diacrylate (PEGDA) hydrogels are also a common hydrogel material used in animal studies.^[44] These hydrogels make a cross-linked network after polymerization with an easily tunable mesh size through modification of PEG chain length between acrylate groups. These hydrogels were also previously used to implant SWCNTs into marine organisms to study implantation

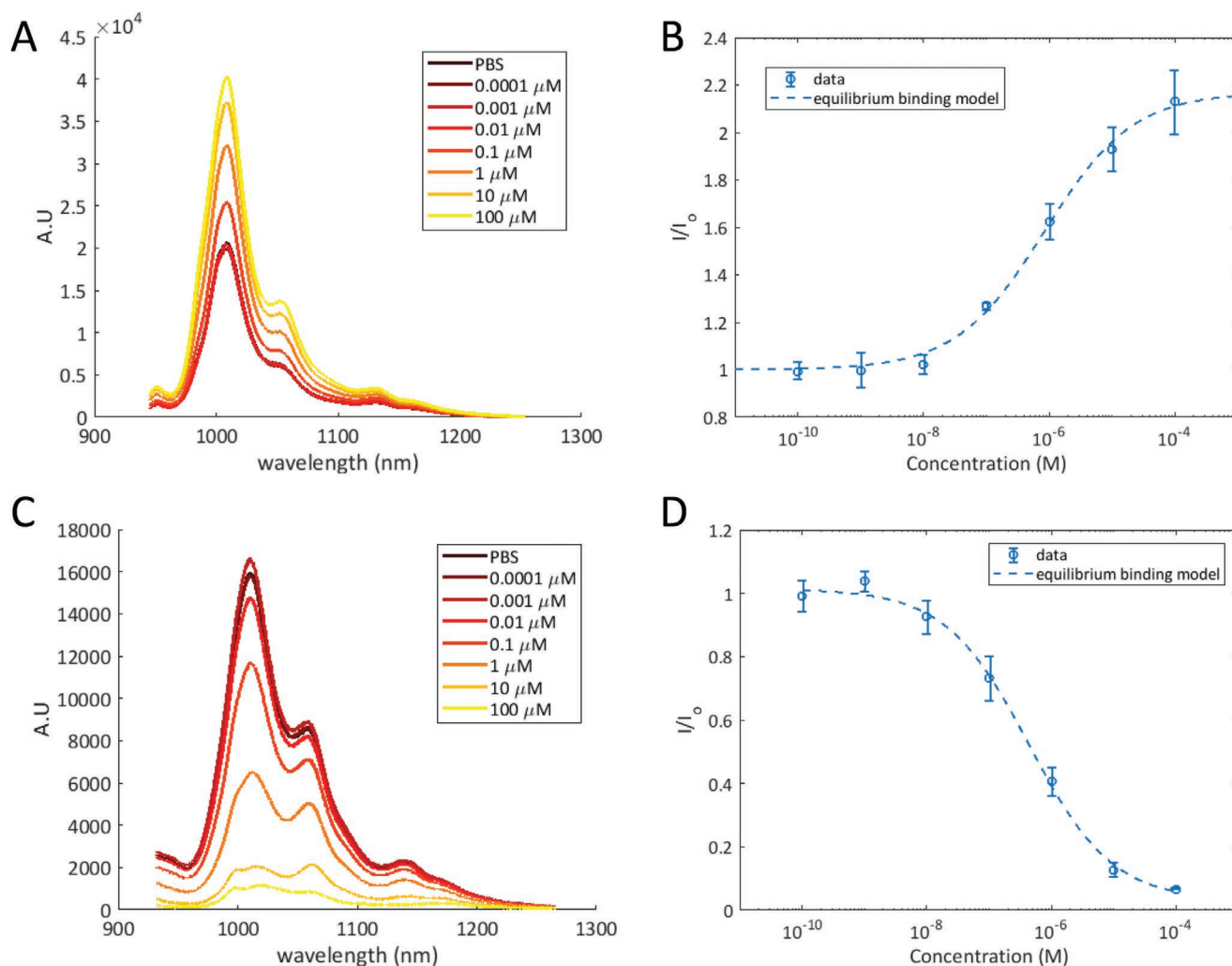


Figure 1. A) Spectral changes of solution phase ex vivo ss(ACCA)₇-SWCNT response to ascorbic acid show significant PL intensity increase. B) Ascorbic acid response calibration curve for ex vivo ss(ACCA)₇-SWCNT. C) Spectral changes of solution phase ex vivo ss(AC)₁₅-SWCNT to riboflavin show significant PL intensity decrease. D) Riboflavin response calibration curve for ex vivo ss(AC)₁₅-SWCNT. (Error bars are standard deviation from three technical replicates.)

depth, fluorescent detection limits, and long-term biocompatibility.^[45] Due to the tunability of the PEGDA system, we choose these hydrogels for our subsequent murine model.

PEGDA hydrogels with embedded sensors are synthesized by first mixing monomer, SWCNT, and initiator. SWCNT sensors were embedded at a concentration of 20 mg L⁻¹. After degassing the mixture under nitrogen, the solution was pipetted in a mold formed by two glass slides separated by spacers (Figure 2A,B). Hydrogels' thickness were chosen between 0.6 and 1 mm to maximize mass transfer while still maintaining enough structure for handling during surgery and implantation. The mass

Table 1. Fitted parameters for solution phase calibration, including 95% confidence interval.

SWCNT	Analyte	n	A	K _D (μM)
(ACCA) ₇	Ascorbic acid	0.62 (0.46, 0.78)	1.17 (1.05, 1.29)	0.86 (0.35, 1.35)
(AC) ₁₅	Riboflavin	0.65 (0.43, 0.87)	-0.98 (-110, -86.3)	0.45 (0.23, 0.68)

transfer characteristics of a number of different hydrogels at different monomer concentrations (in w/v%) were compared, including: Alginate, 3400 Da PEGDA, and 8000 Da PEGDA.

To experimentally study SWCNT leaching over time, 100 μL of gel was incubated in 100 μL of PBS for two days, following which quantification was performed using UV–vis absorbance spectroscopy. Subsequently, the gel was moved to 100 μL of fresh PBS and allowed to incubate for another 4 days for a second-round quantification (Table S2, Supporting Information). Results show that significant leaching occurs in the first 2 days for PEG8000DA gels at 5% and 10% concentration. However, the minimal leaching between 2 and 6 days showed that a pre-leached gel in PBS will maintain a reasonable SWCNT concentration for the duration of our experiment. Thus, we equilibrated gels for 48-h prior to any study.

To test the sensor response within the gel, an imaging baseline was first collected prior to analyte incubation for 15 min. The response of the (ACCA)₇-SWCNT hydrogels to the ascorbic acid after equilibration is shown in Figure 2C. The best performing

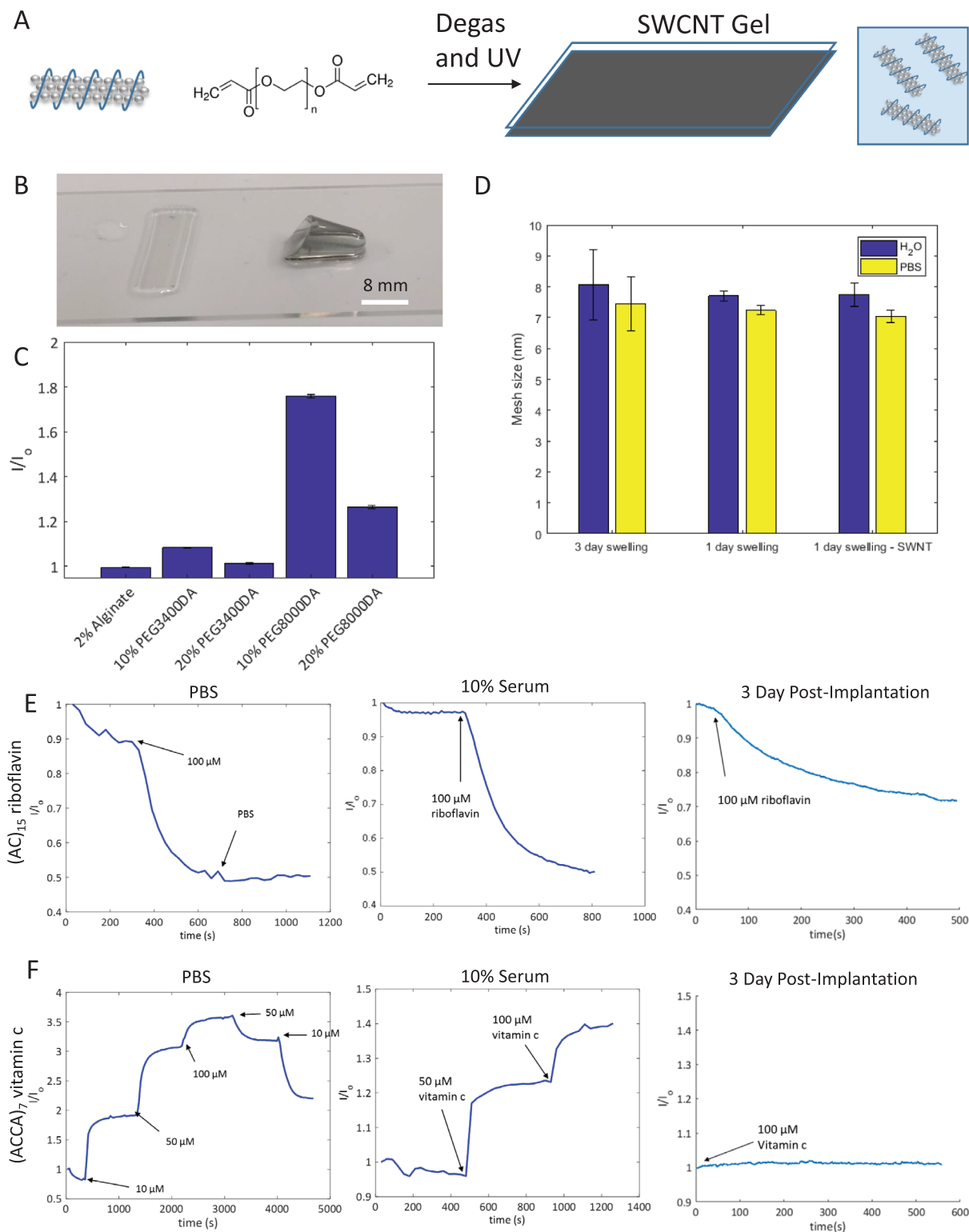


Figure 2. A) Diagram of synthesis of the PEGDA hydrogels; monomer was mixed with SWCNT solution and initiator, was degassed, piped between two glass slides to control for thickness, and exposed to UV light to initiate free radical polymerization. B) Image of SWCNT embedded hydrogels, ratiometric gel (left), and SWCNT hydrogel in tube for visualization (right). C) Measurement of mass transfer characteristics of hydrogels of alginate, PEG3400DA, and PEG8000DA at various (w/v)% monomer concentrations by showing fluorescent response of embedded (ACCA)₇-SWCNT to ascorbic acid after 15 min incubation. D) Characterization of hydrogel mesh size of the best performing 10% (w/v) PEG8000DA hydrogel in the presence of water and PBS with or without SWCNT. E,F) Testing the resistance of the hydrogel and corona phase combination to interferents found in 10% mouse serum and after three days of implantation in vivo. The (AC)₁₅-SWCNT gel shows retained sensor response three days post-implantation, while the (ACCA)₇-SWCNT gel almost loses sensor response entirely.

hydrogel by a significant margin was the 10% (w/v) PEG8000DA that appears to allow analyte diffusion at a reasonable rate.

To further characterize the best performing 10% PEG8000DA gel, the mesh sizes were calculated by swelling measurements in water and PBS with and without SWCNT. The hydrogel mesh size can be calculated using the following equation:^[46,47]

$$\xi = b \left(2 \frac{M_c}{M_r} \right)^{\frac{1}{2}} C_n^{\frac{1}{3}} v_{2,s}^{-\frac{1}{3}} \quad (3)$$

where ξ is the mesh size, b is the bond length (1.5 angstroms), M_r is the molecular weight of the PEG repeating unit (44 Da), C_n is the characteristic ratio for PEG (4) and $v_{2,s}$ is the polymer volume fraction of the hydrogel in the swollen state.

$$v_{2,s} = \frac{1}{Q \frac{\rho_{\text{poly}}}{\rho_{\text{H}_2\text{O}}} + 1} \quad (4)$$

$$Q = \frac{W_{\text{swell}} - W_{\text{dry}}}{W_{\text{dry}}} \quad (5)$$

ρ_{poly} is the density of the polymer (1.12 g cm⁻³), and $\rho_{\text{H}_2\text{O}}$ is the density of water. Q is the swelling ratio and W is the weight of the swollen or dry polymer. The average molecular weight between two crosslinks (M_c) can be calculated using:

$$\frac{1}{M_c} = \frac{2}{M_n} - \frac{1}{V_1} \left[\ln(1 - v_{2,s}) + v_{2,s} + \chi v_{2,s}^2 \right] \quad (6)$$

$$\rho_{\text{poly}} v_{2,s} \left[\left(\frac{v_{2,s}}{v_{2,r}} \right)^{\frac{1}{3}} - \frac{1}{2} \left(\frac{v_{2,s}}{v_{2,r}} \right) \right]$$

where M_n is the number average molecular weight (8000 Da in this case), V_1 is the molar volume of water (18 cm³ mol⁻¹), χ is the Flory–Huggins interaction parameter (0.426 from previous work^[46,47]), $v_{2,r}$ is the volume fraction in the relaxed state, assumed to be the same as in the monomer precursor solution.

The mesh size for various swelling times is shown in Figure 2D and we demonstrate that SWCNT has no effect on the physical crosslinking density of the hydrogel. The mesh size is also only minimally affected by changes in ionic strength. The mesh size is much higher than the hydrodynamic radii of ascorbic acid^[48] and riboflavin,^[49] which was necessary due to the correlation between diffusivity and response time.

The sensing hydrogels and nanosensor combinations were then tested for robustness in the biological environment by either immersing in 10% mouse serum or implanted in a murine model for 3 days (Figure 2E,F). To study sensor response, sensor gels were sandwiched in microfluidic flow chambers and imaged while corresponding buffers containing varying concentrations of analytes flowed past. Data was collected until minimal change was observed after each new analyte condition. Figure 2F demonstrates ascorbic acid sensor reversibility by flowing both increasing and decreasing concentrations of analytes. As the stream was switched from 100 to 50 μM , the sensor response reverted to the previous 50 μM level. Similarly, this was observed when the concentration was changed again to 10 μM . The riboflavin response was not reversible.

For the 3-day post implantation study, the hydrogel was removed and placed in the same flow setup. Analytes were flowed directly without an initial equilibration period to avoid washing away adsorbed interferents (details of the additional 3-day post-implantation saline flow control can be found in the Supporting Information). The (ACCA)₇-SWCNT ascorbic acid sensor shows a diminishing response in the presence of serum while the (AC)₁₅-SWCNT riboflavin does not. Similarly, the 3-day implantations condition showed similar trends with the riboflavin sensor maintaining response while the ascorbic acid sensor became nearly completely attenuated. This is congruent with our previous observation that fibrinogen binding to DNA wrapped SWCNT can decrease “turn on” response SWCNT sensors to analytes such as dopamine.^[50] Combined, these results suggest that protein composition potentially explains the difference between the serum and post-implantation conditions for the ascorbic acid sensor. Due to the robustness of the riboflavin sensor in implantation conditions, it was chosen as the sensor candidate for our following imaging studies regardless of reversibility.

2.3. Ratiometric Sensor Development

When working with an intensity-based sensor, there are a number of mechanical perturbations that can cause method error resulting in spurious changes in fluorescent intensity. These factors include movement, breathing, and fluid level change that can all modify sensor position and thus the optical path-length between the sensing hydrogel and the imaging system.^[38] To account for these factors and increase the signal to noise, an invariance fluorescent marker was used as reference. In this work, we used poly(styrene p-styrenesulfonate), or PSSS, wrapped SWCNT.

PSSS is synthesized using reversible addition fragmentation chain transfer (RAFT) adapted from Liu et al.^[51] A triocetylammmonium hydrochloride (TOA-HCL) was synthesized and used to protect the charged group of a vinyl styrene sulfonate (SS) monomer resulting in SS-TOA. Then the SS-TOA monomer is combined with styrene monomers at 0.363 and 0.637 mole fractions, respectively, in addition to the RAFT agent, 2-(Dodecylthiocarbonothioylthio)-2-methylpropionic acid (RAFT-COOH), and azobisisobutyronitrile (AIBN) as the initiator. This results in a random polymer made of styrene and SS-TOA. Finally, the polymer is deprotected through ion exchange with NaOH resulting in PSSS. Colloidal PSSS-SWCNT is created similarly to other dispersions and encapsulated within the PEGDA hydrogel.

To accomplish spatial ratiometric encoding, we constructed hydrogel pairs where one serves as reference. To eliminate independent movement between the sensor and reference, the two gels are physically coupled by polymerizing together into a combination sensor (Figure 3A). The sensor and reference gels were differentiated by shape. This approach can be easily extended to any spatial pattern or sizing of sensing and reference gels. The sensor response can be corrected using:

$$R_{\text{ratio}} = \frac{R_{\text{sensor}}}{R_{\text{reference}}} = \frac{I_{\text{sensor}}/I_{\text{sensor},o}}{I_{\text{ref}}/I_{\text{ref},o}} \quad (7)$$

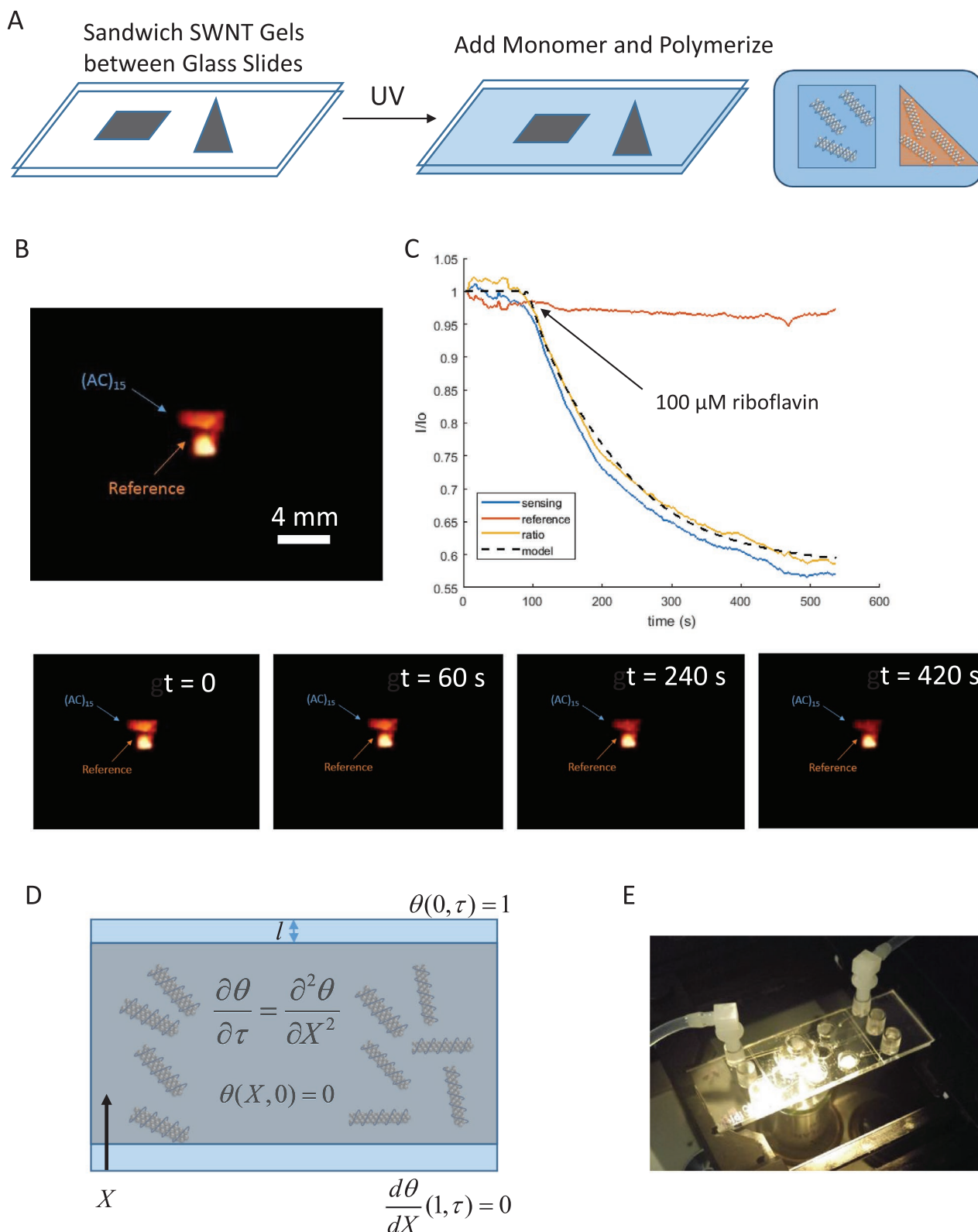


Figure 3. A) Schematic of the procedure for making ratiometric gels where a (AC)₁₅ wrapped SWCNT hydrogel and the invariant polystyrene styrene sulfonate hydrogel are coupled within a single hydrogel. B) Image and video of ratiometric gel showing quenching of sensor gel and constant fluorescence of the reference. C) Fluorescence response of sensor, reference, and ratio which was fit with the diffusion model. D) System of equations for the 1D diffusion model of riboflavin diffusion into the combination hydrogel slab, with a small section without SWCNT to represent the equilibration process. E) Experimental setup for hydrogel flow experiment where the analyte flows both around and above each of the combination gels.

where R_{ratio} is the ratio corrected response, R_{sensor} is the normalized fluorescence of the sensor, I_{sensor} against the baseline, $I_{\text{sensor},0}$ and $R_{\text{reference}}$ is the normalized fluorescence of the reference, I_{ref} against the baseline, $I_{\text{ref},0}$. Figure 3B,C shows both imaging and intensity profile results of the combined gel response of the riboflavin sensor during analyte flow. Flow rate was controlled at the lower limit of 0.3 mL min^{-1} to maintain a constant concentration boundary over the top of the gel.

To characterize the corrected sensor response and gel construction, a 1D mathematical model of analyte diffusion into the sensing gel and equilibrium binding to sensor elements was created to describe the experimental setup (Figure 3D,E). The diffusion model solves the following unsteady diffusion model and boundary conditions:

$$\begin{aligned} \frac{\partial C}{\partial t} &= D \frac{\partial^2 C}{\partial x^2} \\ C(0, x) &= 0 \\ C(t, 0) &= C_0 \\ \frac{dC}{dx}(t, L) &= 0 \end{aligned} \quad (8)$$

where C is the concentration of riboflavin, x is dimension of length, t is time, D is the effective diffusivity in the hydrogel, C_0 is the concentration boundary layer at the top of the gel ($100 \mu\text{m}$ in this case), and L is the thickness of the gel where the no flux condition is maintained (0.1 cm). The system of equations is non-dimensionalized as follows:

$$\begin{aligned} \theta &= \frac{C}{C_0}; X = \frac{x}{L}; \tau = \frac{t}{L^2/D} \\ \frac{\partial \theta}{\partial \tau} &= D \frac{\partial^2 \theta}{\partial X^2} \\ \theta(0, X) &= 0 \\ \theta(\tau, 0) &= 1 \\ \frac{d\theta}{dX}(\tau, 1) &= 0 \end{aligned} \quad (9)$$

where τ is dimensionless time, X is dimensionless distance, and θ is dimensionless concentration. The solution to this dimensionless system of equations is shown below:

$$\begin{aligned} \theta(X, \tau) &= 1 - \sum_{n=0}^{\infty} \frac{2}{\lambda_n} e^{-\lambda_n^2 \tau} \sin \lambda_n X \\ \lambda_n &= \left(n + \frac{1}{2}\right) \pi \text{ where } n = 0, 1, 2, \dots \end{aligned} \quad (10)$$

This solution describes the riboflavin profile across the hydrogel over time. The riboflavin is assumed to have fast kinetics with the SWCNT sensors such that the sensor and the analyte are in equilibrium at all times. Due to the hydrogel thickness being less than the focal volume of the camera lens, PL from imaging is an average of sensor molecule intensities across different gel cross sections. The normalized PL can be calculated from model concentration using integration:

$$\frac{I}{I_0} = \frac{1}{L-2l} \int_l^{L-l} a \frac{C^n}{K_D^n + C^n} + 1 dx \quad (11)$$

Where L is the length of hydrogel and l is the fraction from the surface without SWCNT, thus deducted from the calculation.

Equations (10) and (11) were used to fit the hydrogel fluorescence data as seen in Figure 3C. The K_D and n fitted from the calibration curve. The proportionality constant, a , was allowed to vary as done previously as 2D measurement differs from 1D spectra.^[45] L and l were allowed to vary due to uncertainty in the hydrogel length as well as amount of SWCNT leached. The fit shows that the effective diffusivity of riboflavin in the hydrogel is $8.6 \times 10^{-7} \text{ cm}^2 \text{ s}^{-1}$, which is approximately a third lower than the diffusivity in water and slightly higher than the diffusion of riboflavin in HEMA/MAA copolymer hydrogels without adsorption found by Liu et al.^[49] The fraction of SWCNT-reduced gel from leaching is estimated to be $\approx 16\%$ of the outer length ($a = -0.45$, $L = 0.75 \text{ mm}$). The a is lower than solution phase calibration due to background and hardware changes.

2.4. In Vivo Application

To study our sensor system in an in vivo environment, we performed intraperitoneal (IP) implantation in a murine model. The IP space is an ideal area for implantation due to space availability as well as potential fluid volume, up to 1 mL , for analyte administration. Additionally, IP fluid is an ultrafiltrate of plasma where vitamins and other solutes can be in equilibrium with the rest of the body.^[52] This region is often also used for dialysis removal of solutes from blood.^[53] These properties make it an optimal test location for future systemic detection efforts. Subcutaneous experiments were not considered due to space limitations that can lead to significant errors if the analyte cannot adequately interact with the sensor gel.

Additionally, injections can cause fluid pockets which can spatially alter excitation and emission path length. To prevent this, the mouse is imaged in an inverted fashion through a glass barrier Figure 4A,B. Riboflavin was administered through a catheter implanted in the IP space prior to imaging, which allowed for analyte injection without additional movement or handling. A standoff nIR camera was then focused onto the implantation region. The inverted setup also allowed for tissue compression, which minimizes excessive movement during the experiment. These strategies in combination with the ratiometric hydrogel corrects for many aspects of the method error during our study. The experiment entails gel and catheter implantation followed by an equilibration period of the IP space prior to injection. During imaging measurement, 1 mL of riboflavin or saline were administered through the catheter carefully without perturbing gel position at a known position away. The analyte concentration was increased due to the mostly direction independent nature of the injection, which decreased analyte concentration near the sensors as compared to the flow cell study.

Despite the multiple precautions taken, the necessity of a ratiometric approach is immediately obvious. Figure 4C shows a large jump in both the sensing and reference hydrogels upon injection. Even before analyte administration, small movements can cause large changes in gel PL as observed in Figure 4E. These changes can significantly alter the interpretability of the

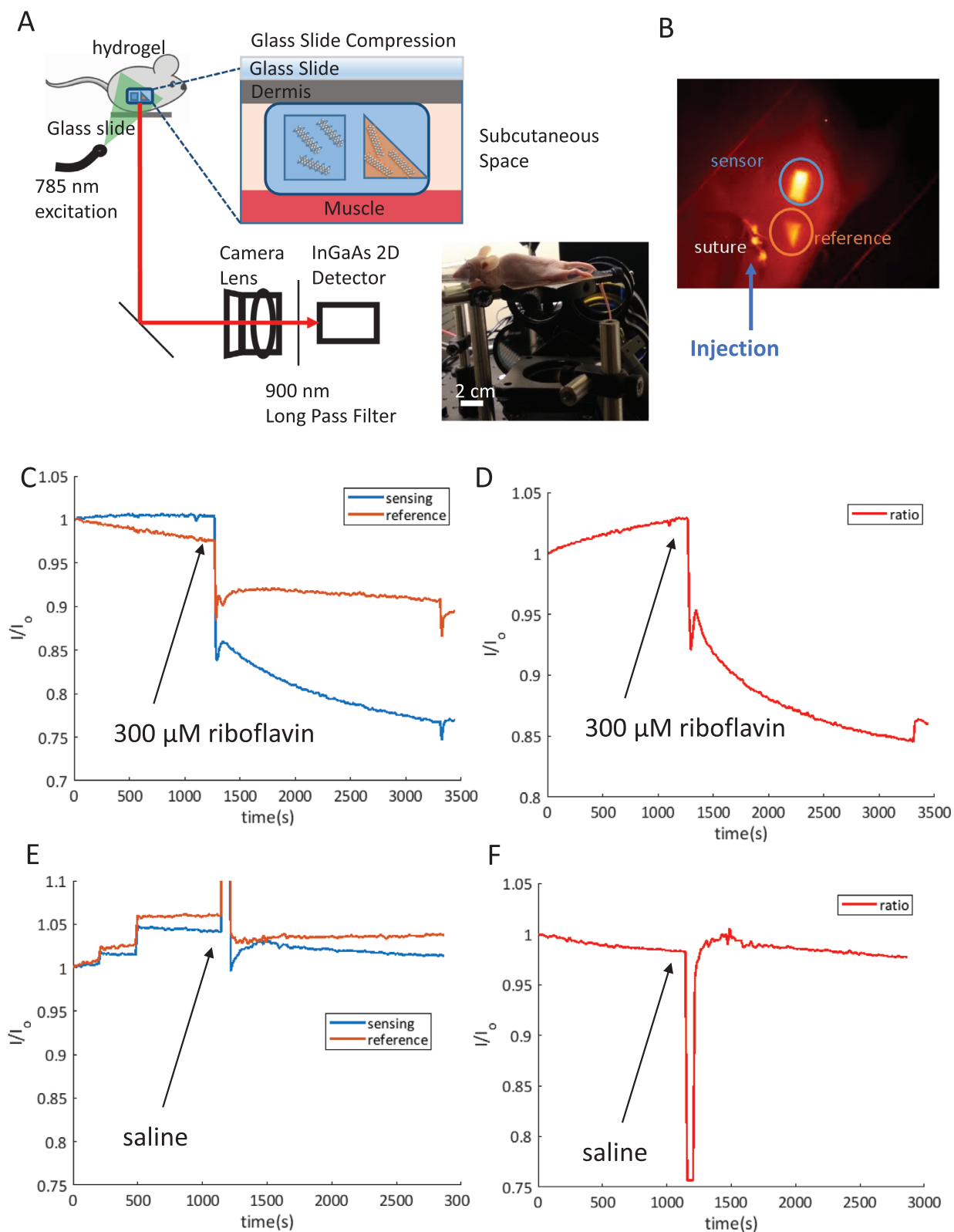


Figure 4. A,B) Schematic of the imaging setup for in vivo experiments. SWCNT hydrogels are imaged through a glass stage to compress the abdomen such that IP catheter injection causes minimal movement. The SWCNT is excited by a 785 nm laser, and the fluorescence is collected through a camera lens and focused onto an InGaAs array. Each implant has a sensor SWCNT hydrogel coupled to a reference for ratiometric measurement. C,D) Sensor intensity and ratiometric corrected profile for experiment with riboflavin injection at 1350s, showing correction of initial jump due to fluid injection. E,F) Sensor intensity and ratiometric corrected profile for experiment with saline injection at 1350s, showing correction of step-wise movement.

Table 2. Equilibration responses (I/I_0) of in vivo experiments for sensor, reference, and ratio hydrogels for mice that were administered riboflavin ($n = 6$) and saline ($n = 3$). ** denotes a p value of <0.005 for a t -test between two conditions.

	Sensor	Reference	Ratio
Saline	0.98 ± 0.03	0.95 ± 0.02	$0.87 \pm 0.05^{**}$
Riboflavin	0.87 ± 0.09	1.00 ± 0.10	$1.01 \pm 0.04^{**}$

results. Using the ratiometric approach, the fluid jump is corrected as seen in Figure 4D. Any drift in the data is smoothed out as seen starkly in the saline control (Figure 4E,F) and corrected ratiometrically. There is a slight drift in the initial ratio response before analyte administration in Figure 4D due to mouse movement resulting in independent movement of sensor versus the reference. However, this moderate 2% drift does not significantly impact the result interpretation. The ratio sensor can correct for cases of significant movement such as seen in Figure 4E,F.

The need for a ratiometric hydrogel is also revealed statistically through technical replicates over different animals for riboflavin ($n = 6$) or saline ($n = 3$) conditions. The final sensor response of each gel is calculated as I/I_0 after 1-h of sensor response equilibration to account for analyte convection, diffusion, and sensor response time. Table 2 shows the data from animal replicates for sensor, reference, and the corrected ratio. Of note, a direct t -test comparison between uncorrected riboflavin and saline control has no significant difference ($p = 0.1$). This is likely due to propagated sources of error across all animals. However, ratiometric corrected data showed significant detection of riboflavin ($p = 0.003$ denoted by **). The orders of magnitude increase in p -value demonstrated significant improvements of a hydrogel ratiometric setup for intensity modulated sensing of fluorescent particles.

3. Conclusion

Herein we present a set of implementation procedures for the sensor system development and the mitigation of error sources for in vivo chemical measurements using intensity-based colloidal fluorescent nanosensors. First, we optimized the SWCNT sensors for response to the analyte of interest. To minimize sensor diffusion error, we created a hydrogel encapsulation scheme. Combining empirical mass transfer studies and modeling, we determined that a 10 (w/v)% PEGDA hydrogel with molecular weight 8000 Da was optimal for sensor particle entrapment and analyte diffusion. After testing the sensor candidates in 10% serum and 3-day implantation, we found the (AC)₁₅-SWCNT maintains its sensor response to riboflavin.

To create a spatial ratiometric system, sensor and analyte invariant reference gels were embedded together into a single sensor. Sensors were implanted into the IP space and measured transcutaneously after a controlled catheter analyte injection. The sensor response ratio allowed for the correction of major sources of error observed, including movement that can significantly affect result interpretation. Statistically, we show that correcting for the noise using a ratiometric approach in each experiment

individually resulted in much more confidence when comparing animal groups. Our ratiometric approach provides an essential roadmap for the implementation of any intensity modulated fluorophore sensor to improve data reliability while performing measurements in already complex in vivo systems.

4. Experimental Section

All materials were purchased from Sigma–Aldrich unless otherwise indicated.

DNA SWCNT Dispersions: HiPCO SWCNT (Nanointegris) or CoMoCat SWCNT (Sigma–Aldrich) was added to 0.1 M NaCl at a concentration of 1 mg mL⁻¹ and the desired DNA (purchased from IDT) was added at a concentration of 2 mg mL⁻¹. The solution, 1 mL final volume, was then sonicated (Qsonica Q125) by a 3 mm probe tip (Cole Palmer) in an ice bath for 15 min at a power of 5 W. The sonicated SWCNT solution was centrifuged (Eppendorf) twice for 90 min at 16 100 relative centrifugal force (RCF) which was used to remove any impurities or aggregates. The supernatant of this solution was collected and characterized using UV–vis–NIR absorption spectroscopy (Shimadzu 3101PC) verifying the presence of sharp absorption peaks for characteristic of separated SWCNTs. The concentration of the final dispersion was calculated by using the absorption at 632 nm and solving Beer–Lambert’s law for concentration using the quartz cuvette (Starna) path length of 1 cm and the extinction coefficient for SWCNT given as $\epsilon_{632\text{nm}} = 0.036 \text{ (mg L}^{-1}\text{)}^{-1} \text{ cm}^{-1}$.^[39]

PSSS Synthesis: Preparation of Trioctylammonium Hydrochloride (TOA–HCl): 20 mL of trioctylamine (TOA, 0.0457 mol) was dissolved in 40 mL hexane and placed in an ice bath. Dropwise addition of 5 mL of concentrated HCl (0.0605 mol) was done while mixing. Solution was stored in freezer for 5 h and white precipitate (trioctylammonium hydrochloride) formed. Filtered precipitate and washed with cold hexane to remove HCl. Product was dried in vacuum oven overnight (16 h) at room temperature. A white solid was obtained.

Preparation of SS-TOA: 10 g TOA–HCl (0.0256 mol) was dissolved in 50 mL dichloromethane. 5.8 g of sodium *p*-styrenesulfonate (0.0282 mol) was dissolved in 40 mL DI water. The solution was mixed in a separation funnel and allowed to settle. The top layer of dichloromethane was collected and washed three times with DI water. The solution was concentrated on a rotary evaporator to obtain a viscous yellow oil, then frozen in a freezer, and finally dried under vacuum overnight to yield a white solid.

PSSS Synthesis: In 10 mL of toluene, the protected SS-TOA was combined with styrene at a 0.363 and 0.637 mole fraction, respectively, with a final monomer concentration of 2.75 M. Additionally, added RAFT–COOH and AIBN (0.12 M and 0.026 M, respectively) and purged with nitrogen for 15 min in an ice bath. Afterward, heated to 80 °C and polymerized for 8 h. What resulted was then added dropwise to cyclohexane to precipitate polymer. Finally, it was deprotected through ion exchange by mixing 50 mg of polymer per 1 mL of toluene with equal volume of 1 M NaOH.

PSSS-SWCNT Dispersions: 5 mg HiPCO SWCNT and 50 mg of polymers were mixed in 5 mL of PBS. The solution was adjusted to a final pH of 7.4 using 2 M NaOH. The mixture was bath sonicated for 10 min and ultrasonicated using a 6 mm probe at a power of 10 W for 1 h (QSonica). The resulting suspension was ultracentrifuged at 155 000 rcf for 4 h. The supernatant was collected and free polymer was removed from the suspension by dialysis against 1x PBS over 5 days using 100 kDa cutoff Float-a-Lyzer devices (Spectrum Labs) with buffer replacements thrice daily. The SWCNT suspensions were characterized as described above.

DNA SWCNT Hydrogel Encapsulation: Hydrogel monomer PEG8000DA (8000 molecular weight polyethylene glycol diacrylate) was purchased from Alfa Aesar. 2-hydroxy-4’-(2-hydroxyethoxy)-2-methylpropiophenone was used as the UV-triggered initiator. The initiator was made into a saturated solution at 7 mg mL⁻¹ in water to add to the monomer solution. SWCNT, at a final concentration of 20 mg L⁻¹,

was added to PEG8000DA monomers, at a final concentration of 10%, in phosphate buffered saline (PBS). Saturated initiator solution was added to the SWCNT/monomer solution at 2.5% (v/v). This solution was then closed in a chamber with N₂ flowing over solution to degas any oxygen in the sample (for 30 min). After degassing the sample, the solution was pipetted in between glass slides separated by a spacer and the slides were put back into the chamber and exposed to UV light (365 nm – 4W) for 30 min to polymerization. After polymerization, the hydrogels were placed in PBS solution to equilibrate for 48 h before testing. For ratiometric hydrogels, shapes of the SWCNT hydrogels were cut and placed between glass slides and filled with degassed monomer and initiator solution (without SWCNT) and polymerized as described above.

nIR Fluorescent Spectra Measurements: The optical setup is discussed in the main body of the paper. In short, a 785 nm laser (450 mW B & W Tek) is connected to a 2 mm achromatic collimator (Thorlabs). The power at the sample is controlled by adding neutral density filters (Thorlabs) in the excitation beam path. The light then bounces off of a 900 nm long pass dichroic mirror (Thorlabs) and is focused through a 2.5 inch working distance f/3.0 noncontact objectives (Kaiser Optical Systems). The light is focused into a quartz cuvette (Starna) that is temperature controlled at 25 °C through a jacket system circulating refrigerant to control the temperature that also allows for a stirbar. The emission is collected after it passes through the 900 nm long pass filter and sent to a PI Acton SP2500 spectrometer and imaged on a liquid nitrogen cooled 1D InGaAs detector (Princeton Instruments).

Standoff Imaging: The wide field of view imaging setup uses a Princeton Instruments OMA V InGaAs detector to capture a 2D image of our mouse with the hydrogel for nIR emissions > 900nm. The detector is cooled to –100 °C using liquid N₂. The detector was affixed with a Nikon AF Micro-Nikkor 60 mm f/2.8D lens to focus the image. A FELH 900 nm long-pass filter (Thorlabs) was placed between the lens and the detector to filter out excitation light. The nanotube embedded hydrogel was excited using a 785 nm Invictus laser with a power density of 20 mW cm⁻². The images obtained by this setup were corrected by subtracting the dark current of the detector at the given exposure time. Images with display were normalized between 0 and 255 for optimal viewing.

Animal Work: All the following procedures performed were approved by the Committee on Animal Care (CAC) and the Division of Comparative Medicine (DCM) at the Massachusetts Institute of Technology (protocol# 0417-035-20). The mice used for this study were SKH1-E mice purchased from Charles River Laboratories. The SKH1-E line is a nude immunocompetent mouse line to simplify imaging of fluorescent implants. All mice were purchased at 6 weeks old and any mice used in this study are between 8–24 weeks of age. For in vivo implantations: hydrogels were sterilized before implantation by illumination with UV light for 30 min. A 10 x 10 mm piece of hydrogel was implanted into the intraperitoneal space through a ventral incision. A 2.5" catheter was implanted in the intraperitoneal space through the same incision. The abdominal muscles and skin were closed using sutures. Prior to the operation, the mouse was anesthetized using 2% isoflurane gas and held under for the remainder of the surgery and the subsequent imaging. Additionally, analgesics were administered prior to implantation. During imaging, 1 mL of 300 μM riboflavin (or saline for controls) was injected into the intraperitoneal space through the catheter after collecting fluorescent baseline for 5 min. Data was collected for 1-h post injection.

Supporting Information

Supporting Information is available from the Wiley Online Library or from the author.

Conflict of Interest

The authors declare no conflict of interest.

Data Availability Statement

The data that support the findings of this study are available from the corresponding author upon reasonable request.

Keywords

carbon nanotubes, in vivo, sensors, vitamins

Received: January 27, 2021

Revised: April 29, 2021

Published online: June 27, 2021

- [1] D. J. Brenner, E. J. Hall, *N. Engl. J. Med.* **2007**, *357*, 2277.
- [2] A. F. Fercher, W. Drexler, C. K. Hitzenberger, T. Lasser, *Rep. Prog. Phys.* **2003**, *66*, 239.
- [3] U. Vovk, F. Pernus, B. Likar, *IEEE Trans. Med. Imaging* **2007**, *26*, 405.
- [4] D. R. Thevenot, *Pure Appl. Chem.* **1999**, *71*, 2333.
- [5] M. N. Velasco-Garcia, *Semin. Cell Dev. Biol.* **2009**, *20*, 27.
- [6] C. I. L. Justino, T. A. Rocha-Santos, A. C. Duarte, *Trends Anal. Chem.* **2010**, *29*, 1172.
- [7] B. Linke, W. Kerner, M. Kiwit, M. Pishko, A. Heller, *Biosens. Bioelectron.* **1994**, *9*, 151.
- [8] T. Ohara, R. Rajagopalan, A. Heller, *Anal. Chem.* **1994**, *66*, 2451.
- [9] R. M. Bergenstal, W. V. Tamborlane, A. Ahmann, J. B. Buse, G. Dailey, S. N. Davis, C. Joyce, T. Peoples, B. A. Perkins, J. B. Welsh, S. M. Willi, M. A. Wood, *N. Engl. J. Med.* **2010**, *363*, 311.
- [10] M. A. Lee, S. Wang, X. Jin, N. A. Bakh, F. T. Nguyen, J. Dong, K. S. Sillmore, X. Gong, C. Pham, K. K. Jones, S. Muthupalani, G. Bisker, M. Son, M. S. Strano, *Adv. Healthcare Mater.* **2020**, *9*, 2000429.
- [11] S. Bhattacharya, X. Gong, E. Wang, S. K. Dutta, J. R. Caplette, M. Son, F. T. Nguyen, M. S. Strano, D. Mukhopadhyay, *Cancer Res.* **2019**, *79*, 4515.
- [12] E. J. Llorent-Martínez, J. F. García-Reyes, P. Ortega-Barrales, A. Molina-Díaz, *Anal. Chim. Acta* **2006**, *555*, 128.
- [13] L. García, S. Blázquez, M. P. San Andrés, S. Vera, *Anal. Chim. Acta* **2001**, *434*, 193.
- [14] D. S. Bhat, L. L. Gruca, C. D. Bennett, P. Katre, A. V. Kurpad, C. S. Yajnik, S. C. Kalhan, *PLoS One* **2018**, *13*, e0196970.
- [15] M. J. Ramalho, M. A. N. Coelho, M. C. Pereira, in *A Critical Evaluation of Vitamin D - Clinical Overview*, IntechOpen Limited, London, U.K **2017**, Ch.11.
- [16] C.-Y. Hsu, P.-W. Wang, A. Alalaiwe, Z.-C. Lin, J.-Y. Fang, *Nutrients* **2019**, *11*, 68.
- [17] P. W. Barone, R. Parker, M. S. Strano, *Anal. Chem.* **2005**, *77*, 7556.
- [18] A. a. Boghossian, J. Zhang, P. W. Barone, N. F. Reuel, J.-H. Kim, D. a. Heller, J.-H. Ahn, A. J. Hilmer, A. Rwei, J. R. Arkalgud, C. T. Zhang, M. S. Strano, *ChemSusChem* **2011**, *4*, 848.
- [19] P. V. Jena, T. V. Galassi, D. Roxbury, D. A. Heller, *ECS J. Solid State Sci. Technol.* **2017**, *6*, M3075.
- [20] A. M. Smith, M. C. Mancini, S. Nie, *Nat. Nanotechnol.* **2009**, *4*, 710.
- [21] D. A. Heller, S. Baik, T. E. Eurell, M. S. Strano, *Adv. Mater.* **2005**, *17*, 2793.
- [22] A. V. Venediktova, V. N. Bocharov, A. Y. Vlasov, I. M. Kislyakov, V. M. Kiselev, E. A. Kats, E. D. Obratsova, A. S. Pozharov, S. A. Povarov, *Opt. Spectrosc.* **2014**, *116*, 418.
- [23] J. Zhang, M. P. Landry, P. W. Barone, J. Kim, *Nat. Nanotechnol.* **2013**, *8*, 959.
- [24] H. Jin, D. a. Heller, M. Kalbacova, J.-H. Kim, J. Zhang, A. a. Boghossian, N. Maheshri, M. S. Strano, *Nat. Nanotechnol.* **2010**, *5*, 302.

- [25] J. H. Kim, C. R. Patra, J. R. Arkalgud, A. A. Boghossian, J. Zhang, J. H. Han, N. F. Reuel, J. H. Ahn, D. Mukhopadhyay, M. S. Strano, *ACS Nano* **2011**, *5*, 7848.
- [26] J. Zhang, A. A. Boghossian, P. W. Barone, A. Rwei, J. H. Kim, D. Lin, D. A. Heller, A. J. Hilmer, N. Nair, N. F. Reuel, M. S. Strano, *J. Am. Chem. Soc.* **2011**, *133*, 567.
- [27] E. Polo, S. Kruss, *J. Phys. Chem. C* **2016**, *120*, 3061.
- [28] S. Kruss, M. P. Landry, E. Vander Ende, B. M. Lima, N. F. Reuel, J. Zhang, J. Nelson, B. Mu, A. Hilmer, M. Strano, *J. Am. Chem. Soc.* **2014**, *136*, 713.
- [29] A. G. Beyene, A. A. Alizadehmojarad, G. Dorlhiac, N. Goh, A. M. Streets, P. Král, L. Vuković, M. P. Landry, *Nano Lett.* **2018**, *18*, 6995.
- [30] T. V. Galassi, P. V. Jena, J. Shah, G. Ao, E. Molitor, Y. Bram, A. Frankel, J. Park, J. Jessurun, D. S. Ory, A. Haimovitz-Friedman, D. Roxbury, J. Mittal, M. Zheng, R. E. Schwartz, D. A. Heller, *Sci. Transl. Med.* **2018**, *10*, eaar2680.
- [31] J. D. Harvey, P. V. Jena, H. A. Baker, G. H. Zerze, R. M. Williams, T. V. Galassi, D. Roxbury, J. Mittal, D. A. Heller, *Nat. Biomed. Eng.* **2017**, *1*, 0041.
- [32] G. Bisker, J. Dong, H. D. Park, N. M. Iverson, J. Ahn, J. T. Nelson, M. P. Landry, S. Kruss, M. S. Strano, *Nat. Commun.* **2016**, *7*, 10241.
- [33] G. Bisker, N. A. Bakh, M. A. Lee, J. Ahn, M. Park, E. B. O. Connell, N. M. Iverson, M. S. Strano, *ACS Sens.* **2018**, *3*, 367.
- [34] M. H. Wong, J. P. Giraldo, S. Y. Kwak, V. B. Koman, R. Sinclair, T. T. S. Lew, G. Bisker, P. Liu, M. S. Strano, *Nat. Mater.* **2017**, *16*, 264.
- [35] A. G. Beyene, K. Delevich, J. T. Del Bonis-O'Donnell, D. J. Piekarski, W. C. Lin, A. W. Thomas, S. J. Yang, P. Kosillo, D. Yang, G. S. Prounis, L. Wilbrecht, M. P. Landry, *Sci. Adv.* **2019**, *5*, eaaw3108.
- [36] N. M. Iverson, P. W. Barone, M. Shandell, L. Trudel, S. Sen, F. Sen, V. Ivanov, E. Atolia, E. Farias, T. P. McNicholas, N. Reuel, N. M. A. Parry, G. N. Wogan, M. S. Strano, *Nat. Nanotechnol.* **2013**, *8*, 873.
- [37] T. V. Galassi, M. Antman-Passig, Z. Yaari, J. Jessurun, R. E. Schwartz, D. A. Heller, *PLoS One* **2020**, *15*, e0226791.
- [38] R. Weigert, M. Sramkova, L. Parente, P. Amornphimoltham, A. Masedunskas, *Histochem. Cell Biol.* **2010**, *133*, 481.
- [39] N. M. Iverson, M. S. Strano, G. N. Wogan, *Curr. Protoc. Chem. Biol.* **2016**, *7*, 93.
- [40] G. Yang, C. Sau, W. Lai, J. Cichon, W. Li, *Chem. Soc. Rev.* **2015**, *344*, 1173.
- [41] J. P. Giraldo, M. P. Landry, S.-Y. Kwak, R. M. Jain, M. H. Wong, N. M. Iverson, M. Ben-Naim, M. S. Strano, *Small* **2015**, *11*, 3973.
- [42] D. P. Salem, X. Gong, A. T. Liu, V. B. Koman, J. Dong, M. S. Strano, *J. Am. Chem. Soc.* **2017**, *139*, 16791.
- [43] X. Gong, A. K. Sharma, M. S. Strano, D. Mukhopadhyay, *ACS Nano* **2014**, *8*, 9126.
- [44] M. Choi, M. Humar, S. Kim, S. Yun, *Adv. Mater.* **2015**, *27*, 4081.
- [45] M. A. Lee, F. T. Nguyen, K. Scott, N. Y. L. Chan, N. A. Bakh, K. K. Jones, C. Pham, P. Garcia-Salinas, D. Garcia-Parraga, A. Fahlman, V. Marco, V. B. Koman, R. J. Oliver, L. W. Hopkins, C. Rubio, R. P. Wilson, M. G. Meekan, C. M. Duarte, M. S. Strano, *ACS Sens.* **2019**, *4*, 32.
- [46] A. Cavallo, M. Madaghiele, U. Masullo, M. G. Lionetto, A. Sannino, *J. Appl. Polym. Sci.* **2017**, *134*, 44380.
- [47] N. A. Peppas, H. J. Moynihan, L. M. Lucht, *J. Biomed. Mater. Res.* **1985**, *19*, 397.
- [48] M. Shamim, S. M. A. Baki, *Aust. J. Chem.* **1980**, *33*, 1857.
- [49] D. E. Liu, T. J. Dursch, N. O. Taylor, S. Y. Chan, D. T. Bregante, C. J. Radke, *J. Controlled Release* **2016**, *239*, 242.
- [50] R. L. Pinals, D. Yang, A. Lui, W. Cao, M. P. Landry, *J. Am. Chem. Soc.* **2020**, *142*, 1254.
- [51] Y. Liu, K. L. Pollock, K. A. Cavicchi, *Polymer* **2009**, *50*, 6212.
- [52] M. F. Sorrell, O. Frank, H. Aquino, A. D. Thomson, M. M. Howard, H. Baker, *Am. J. Clin. Nutr.* **1972**, *25*, 125.
- [53] R. Mehrotra, O. Devuyt, S. J. Davies, D. W. Johnson, *J. Am. Soc. Nephrol.* **2016**, *27*, 3238.